Evaporation Heat Transfer and Pressure Drop Characteristics of R-134a in the Oblong Shell and Plate Heat Exchanger

Jae-Hong Park*
Department of Refrigeration & Air-Conditioning Engineering, PuKyong National University, San 100, Yong-dang dong, Namgu, Busan 608-739, Korea
Young-Soo Kim
College of Engineering School of Mechanical Engineering, PuKyong National University, San 100, Yong-dang dong, Namgu, Busan 608-739, Korea

The evaporation heat transfer coefficient h_r and frictional pressure drop Δp_f of refrigerant R-134a flowing in the oblong shell and plate heat exchanger were investigated experimentally in this study. Four vertical counterflow channels were formed in the oblong shell and plate heat exchanger by four plates of geometry with a corrugated sinusoid shape of a 45° chevron angle. Upflow of refrigerant R-134a boils in two channels receiving heat from downflow of hot water in other channels. The effects of the refrigerant mass flux, average heat flux, refrigerant saturation temperature and vapor quality of R-134a were explored in detail. Similar to the case of a plate heat exchanger, even at a very low Reynolds number, the flow in the oblong shell and plate heat exchanger remains turbulent. The results indicate that the evaporation heat transfer coefficient h_r and pressure drop Δp_f increase with the vapor quality. A rise in the refrigerant mass flux causes an increase in the h_r and Δp_f. But the effect of the average heat flux does not show significant effect on the h_r and Δp_f. Finally, at a higher saturation temperature, both the h_r and Δp_f are found to be lower. The empirical correlations are also provided for the measured heat transfer coefficient and pressure drop in terms of the Nusselt number and friction factor.

Key Words : Oblong Shell and Plate Heat Exchanger, Evaporation, Heat Transfer Coefficient, Pressure Drop

Nomenclature

A : Heat transfer area of the plate [m^2]
b : Channel spacing [m]
Bo : Boiling number
c_p : Specific heat [J/kgK]
D_h : Hydraulic diameter [m]
f : Friction factor
G : Mass flux [kg/m^2s]
h : Heat transfer coefficient [W/m^2K]
i_{fg} : Enthalpy of vaporization [J/kg]
k : Conductivity [W/mK]
L : Length from center of inlet port to center of exit port [m]
m : Mass flow rate [kg/s]
Nu : Nusselt number
Pr : Prandtl number
Q : Heat transfer rate [W]
Re : Reynolds number
T : Temperature [℃]
U : Overall heat transfer coefficient [W/m^2K]
u : Velocity [m/s]
x : Vapor quality

Greek Letters

Δp : Pressure drop [Pa]
ΔT : Temperature difference [K]
μ : Viscosity [Ns/m^2]

* Corresponding Author,
E-mail : parksonforever@hanmail.net
TEL : +82-51-620-1503; **FAX** : +82-51-623-8495
Department of Refrigeration & Air-Conditioning Engineering, PuKyong National University, San 100, Yong-dang dong, Namgu, Busan 608-739, Korea. (Manuscript **Received** May 24, 2004; **Revised** August 24, 2004)

ρ : Density [kg/m^3]
v : Specific volume [m^3/kg]

Subscripts

eq : Equivalent
i, o : inlet and exit
l : Liquid
lat : Latent heat
p : Pre-heater
r : Refrigerant
sat : Saturation
$sens$: Sensible heat
t : Test section
tp : Two-phase
v : Vapor
w : Water

1. Introduction

For the last few decades, there has been tremendous advancement in the manufacturing technology of high efficiency heat exchangers. This has allowed the use of smaller and high performance heat exchangers. Consequently, the use of smaller and high performance heat exchanger has become popular in the design of HVAC heat exchangers. Normally, these heat exchangers are used in the two phase system for evaporation and condensation. In the design and analysis of the two phase system within this heat exchanger, it is necessary to understand the heat transfer and frictional characteristics of the heat exchanger.

When compared with the well-established shell-and-tube heat exchangers, the plate heat exchanger shows a number of advantages. Wherever a close temperature approach is required, weight or space is at a premium or corrosion-resistant materials such as stainless steel or titanium are needed, the plate heat exchanger becomes the prime candidate for heat exchanger selection. It is also used widely as a steam heater, as an evaporator, as part of air-conditioning plants in large buildings, as a wet gas cooler, and more recently in refrigeration plants. The significant advantages are given below.

The general trend of increasing energy cost and the need to conserve energy resources require high heat recoveries in heat exchangers. The plate heat exchanger attains high heat transfer coefficients and basically operates with full counter-current flow, enabling small end temperature differences. In a recuperative interchange, this is equivalent to 86% heat recovery. In a tubular heat exchanger, liquid holdup compared with the surface area is large. In a plate heat exchanger, use of rectangular channels with narrow gaps leads to a compact construction and low liquid holdup. This feature is enhanced by the high heat transfer coefficients, which reduce the surface area requirements compared with a shell-and-tube exchanger. Added advantages of the low holdup are low weight and a short start-up time. Because the high heat transfer coefficients in a plate heat exchanger are generated by turbulence, the surface shear stresses are very high, allowing a high fouling removal rate. Compare with the shell and tube, fouling resistances are very low for most types of fouling.

The oblong shell and plate heat exchanger is an interesting variant on the conventional plate heat exchanger. The plates that have an oblique pattern are ellipse in shape, and stacked together in criss-cross arrangements, which are enclosed in a cylindrical shell. The operating temperature may rise up to 350℃, and the pressure up to 10 MPa can be sustained. Although oblong shell and plate heat exchanger is different from the conventional rectangular plate heat exchanger, the underlying flow channels through the exchanger are the same as those in the conventional plate heat exchanger. Therefore, oblong shell and plate heat exchanger is being introduced to refrigeration and air conditioning systems as condensers or evaporators for their high efficiency and compactness. However, there are little data available for the design of oblong shell and plate heat exchanger used as condensers and evaporators.

In this study, the characteristics of the evaporation heat transfer and pressure drop for refrigerant R-134a flowing in the oblong shell and plate heat exchanger were explored experimentally. Before examining the flow boiling characteristics, a preliminary experiment for measuring water-to-water single-phase convection heat

transfer in the oblong shell and plate heat exchanger was performed. The modified Wilson plot method (Farrell et al., 1991) was adopted to calculate the relation between the single-phase convection heat transfer coefficient and flow rate from the measured data. This single-phase heat transfer coefficient was used to analyze the data acquired from the two-phase heat transfer experiments.

2. Experimental Apparatus and Procedure

The experimental system and heat transfer plate used to investigate the evaporation heat transfer characteristics of R-134a are shown in Figs. 1 and 2, respectively. The detailed configurations of the oblong and shell plate heat exchanger are given in Table 1. The experimental system consisted of a test section, a refrigerant loop, a water loop and a data acquisition unit.

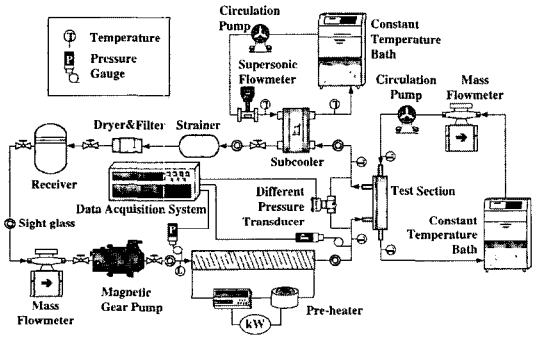

Fig. 1 Schematic diagram of experimental system

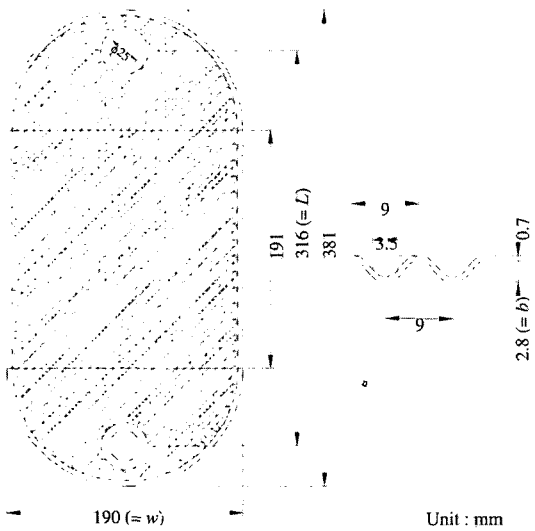

Fig. 2 Schematic diagram of heat transfer plate of oblong shell and plate heat exchanger

2.1 Test section

Figure 3 shows the flow direction in the oblong shell and plate heat exchanger. Four vertical counterflow channels were formed by four corrugated plates of sinusoid pattern with a 45° chevron angle. The upflow of R-134a boils by receiving heat from downflow of hot water. Refrigerant R-134a is circulated in the refrigerant loop. In order to obtain different test conditions of R-134a including the vapor quality, saturation temperature (pressure) and heat flux, the temperatures and flow rate of the working fluid in the water loop were controlled.

Table 1 Configurations of oblong shell and plate heat exchanger

Plate material	SUS 304
Shell material	Steel
Plate length [m]	0.381
Port diameter [m]	0.025
Pitch between plates [m]	0.0028
Plate thickness [m]	0.0007
Max. working pressure [MPa]	10
Category temperature range [℃]	−196~400
Surface per plate [m^2]	0.073
Chevron angle [°]	45

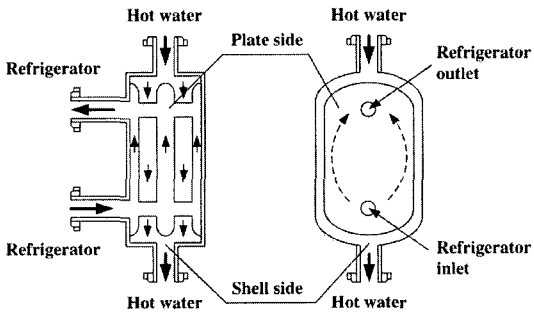

Fig. 3 Details of flow direction

2.2 Refrigerant loop

The refrigerant loop contains a refrigerant pump, a refrigerant flow meter, a pre-heater, a test section (oblong shell and plate heat exchanger), a sub-cooler, a receiver, a strainer, a dryer/filter and sight glasses. The refrigerant pump is a magnetic pump (TUTHILL California) driven by a DC motor which is, in turn, controlled by a variable DC output motor controller. The R-134a flow rate was controlled by the rotational speed of DC motor through the change of DC current. The refrigerant flow rate was measured by a mass flow meter (Oval) installed between the pump and receiver with an accuracy of $\pm 0.2\%$.

The pre-heater is used to evaporate the refrigerant to a specified vapor quality at the test section inlet. Note that the amount of heat transfer from the pre-heater to refrigerant is measured by a power meter (YOKOGAWA) connected to the pre-heater source. The dryer/filter intends to filter the solid particles possibly present in the loop. Meanwhile, a sub-cooler was used to condense the refrigerant vapor flowing out the test section by a cold water to avoid cavitations at the pump inlet. The pressure of the refrigerant loop was controlled by varying the temperature and flow rate of cold water in the sub-cooler. After condensed, the subcooled liquid refrigerant flows back to the receiver.

2.3 Water loop for test section

The water loop in the system, which is designated for circulating hot water through the test section, has a 200 liter constant temperature water bath equipped with a 5 kW heater and an air cooled refrigeration unit of 1 RT cooling capacity. The hot water is driven by a 0.37 kW water pump with an inverter. The accuracy of water flow rate measurement by the mass flow meter is $\pm 0.2\%$.

2.4 Water loop for sub-cooler

The water loop for condensing the R-134a vapor has a 200 liter constant temperature water bath equipped with a 5 kW heater and an air cooled refrigeration unit of 3 RT cooling capacity. A 0.37 kW water pump with an inverter is used to drive the cold water at a specified water flow rate to the sub-cooler. The supersonic flow meter to measure water flow rate has an accuracy of $\pm 1\%$.

2.5 Data acquisition

The data acquisition unit includes a 20 channel NetDAQ 2640A recorder of FLUKE combined with a personal computer. The recorder was used to record the temperature and voltage data. The water flow meter and pressure transducer and differential pressure transducer output voltage of 0~10 V. The NetDAQ 2640A recorder allows the measured data to transmit to personal computer and then to be analyzed by the computer immediately.

2.6 Experimental procedures

In each test, the system pressure is maintained at a specified level by adjusting the water loop temperature and its flow rate. The vapor quality of R-134a at the test section inlet was kept at the desired value by the pre-heater. Finally, the heat transfer rate between the counterflow channels in the test section can be varied by changing the temperature and flow rate in the water loop. Any change of the system variables will lead to fluctuations in the temperature and pressure of the flow. It takes about 60 min to reach a statistically steady state at which variations of mass flux are less than 3% and the variations of the saturation temperature and heat flux are within 3% and 5%, respectively. Then the data acquisition unit is initiated to scan all the data channels for 60 times in 5 minutes. The mean values of the data for all channels are obtained to calculate the heat transfer coefficient.

3. Data Reduction

3.1 Two phase evaporation heat transfer

From the definition of the hydraulic diameter, Shah and Wanniarachchi (1992) suggested to use two times of the channel spacing as the hydraulic diameter for plate heat exchangers when the channel width is much larger than the channel

spacing. So we follow this suggestion.

$$D_n \approx 2b = 0.0056m \tag{1}$$

The total heat transfer rate between the counterflows in the test section is calculated from the hot water side as

$$Q_t = m_w c_{p,w}(T_{w,i} - T_{w,o}) \tag{2}$$

Then, the refrigerant vapor quality entering the test section is evaluated from the energy balance for the pre-heater. The heat transfer to the refrigerant in the pre-heater is the sum of sensible heat transfer (for the temperature rise of refrigerant to the saturated value) and latent heat transfer (for the evaporation of refrigerant).

$$Q_p = Q_{sens} + Q_{lat} \tag{3}$$

Where

$$Q_{sens} = m_r c_{p,r}(T_{r,sat} - T_{r,p,i}) \tag{4}$$

$$Q_{lat} = m_r i_{fg} x_{p,o} \tag{5}$$

The above equations are combined to evaluate the refrigerant quality at the exit of pre-heater that is considered to be the same as the vapor quality of refrigerant entering the test section. Specifically,

$$x_i = x_{p,o} = \frac{1}{i_{fg}}\left(\frac{Q_p}{m_r} - c_{p,r}(T_{r,sat} - T_{r,p,i})\right) \tag{6}$$

The change in the refrigerant vapor quality in the test section is then deduced from the heat transfer to the refrigerant in the test section,

$$\Delta x = \frac{Q_t}{m_r \cdot i_{fg}} \tag{7}$$

The average quality in the test section is given as

$$x_m = x_i + \frac{\Delta x}{2} \tag{8}$$

The overall heat transfer coefficient U for the counterflow between the two channels can be expressed as

$$U = \frac{Q_t}{A \cdot LMTD} \tag{9}$$

where $LMTD$ is the logarithmic mean temperature difference between the two channels defined as

$$LMTD = \frac{(\Delta T_1 - \Delta T_2)}{\ln(\Delta T_1 / \Delta T_2)} \tag{10}$$

Where

$$\Delta T_1 = T_{w,i} - T_{r,sat,o} \tag{11}$$

$$\Delta T_2 = T_{w,o} - T_{r,sat,i} \tag{12}$$

and $T_{r,sat,i}$ and $T_{r,sat,o}$ are the saturation temperatures of R-134a corresponding respectively to the inlet and outlet pressures in the test section. In view of the same heat transfer area in the refrigerant and water sides, the relation between the overall heat transfer coefficient and the convective heat transfer coefficients on both sides can be expressed as

$$\left(\frac{1}{h_r}\right) = \left(\frac{1}{U}\right) - \left(\frac{1}{h_w}\right) - R_{wall}A \tag{13}$$

where the modified Wilson plot method (Farrell et al., 1991) was applied to calculate h_w. In this method, shell side heat transfer correlation is assumed to be that of Sieder-Tate (1936) type and exponent of the Reynolds number and proportional constant are determined from the experimental data. Experiments are conducted varying the shell side flow rate with the plate side flow rate and the temperature fixed. This method is known to have advantage over the original Wilson plot (1915) that smaller numbers of test runs are needed. One should be cautious to make both sides of the flow turbulent.

3.2 Two phase frictional pressure drop

The frictional pressure drop Δp_f was calculated by subtracting the acceleration pressure drop Δp_a, the pressure drop at the test section inlet and exit ports Δp_{port}, and the elevation pressure drop Δp_{ele} from the measured total pressure drop Δp_{exp} for the refrigerant channel.

$$\Delta p_f = \Delta p_{exp} - \Delta p_a - \Delta p_{ele} - \Delta p_{port} \tag{14}$$

The acceleration and elevation pressure drop were estimated as

$$\Delta p_a = -\Delta\left[\frac{G^2 x^2}{\alpha \rho_v} + \frac{G^2(1-x)^2}{(1-\alpha)\rho_l}\right] \tag{15}$$

$$\Delta p_{ele} = [(1-\alpha)\rho_l + \alpha\rho_v]gL \tag{16}$$

Where α is void fraction defined by Zivi (1964).

The pressure drop in the inlet and exit ports was empirically suggested by Shah and Focke

(1988). It is approximately 1.5 times the head due to the flow expansion at the channel inlet

$$\Delta p_{port}=1.5\left(\frac{u_m^2}{2v_m}\right) \tag{17}$$

where u_m is the mean flow velocity. With the homogeneous model, the mean velocity is

$$u_m=Gv_m \tag{18}$$

Based on the above estimation, the acceleration pressure drop, the pressure drop at the test section inlet and exit ports, and the elevation pressure drop were found to be rather small. The frictional pressure drop ranges from 95% to 99% of the total measured pressure drop. According to the definition

$$f_{tp}\equiv-\frac{\Delta p_f D_h}{2G^2 v_m L} \tag{19}$$

the frictional factor for the evaporation of R-134a is obtained.

4. Results and Discussion

4.1 Single phase heat transfer

Before measuring the R-134a evaporation heat transfer, single phase water-to-water tests were conducted first. The results from this single phase experiment are illustrated Fig. 4, and the measured convection heat transfer coefficient in the shell side was correlated by the least square method as

$$Nu_s=0.05\mathrm{Re}^{0.95}\mathrm{Pr}^{1/3} \tag{20}$$

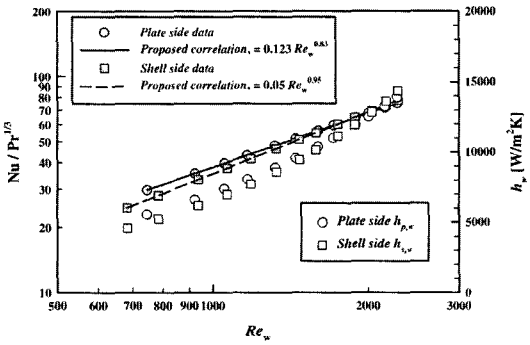

Fig. 4 Heat transfer coefficient variations with the Reynolds number for the shell side in single phase water-to-water test

The energy balance between the hot and cold side of water was within 5% for all runs. To estimate the uncertainty of single phase heat transfer coefficient, an uncertainty analysis proposed by Kline and McClintock (1953) was carried out. The uncertainty of single phase heat transfer coefficient was within about ±10%.

4.2 Two phase evaporation heat transfer

In the present investigation, the mass flux G was varied from 40 to 80 kg/m^{2}s, the average heat flux q_w'' from 4.0 to 8.0 kW/m^2 and the saturation temperature $T_{r,sat}$ from 0 to 10℃. The measured heat transfer coefficients are to be presented in terms of their variations with the average vapor quality in the test section.

Figure 5 shows the effect of refrigerant mass flux on the measured evaporation heat transfer coefficient, where the measured data for G=40, 60 and 80 kg/m^{2}s at $T_{r,sat}$=10℃ and q_w''=6.0 kW/m^2 is plotted as a function of x_m. The results show that the evaporation heat transfer coefficient rises with the mass flux, and for the higher mass flux, the heat transfer coefficient rises more quickly than that for the lower mass flux. This is attributed to the fact that, at 10℃, the liquid density of R-134a is about 62 times the corresponding vapor density. Thus, a large increase in the vapor volume during the evaporation process causes the vapor flow to move at high

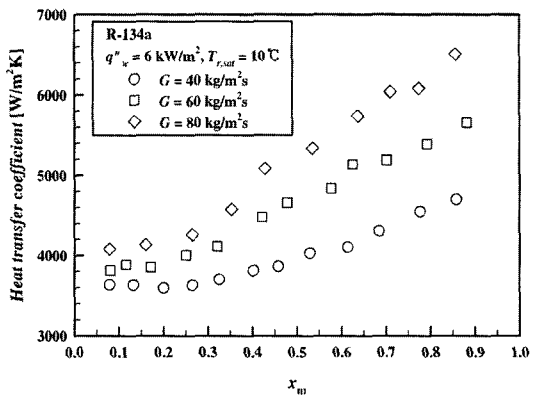

Fig. 5 Variation of evaporation heat transfer coefficient with mean vapor quality for various mass fluxes at q_w''=6 kW/m^2 and $T_{r,sat}$= 10℃

speed, which in turn breaks the adjacent liquid film into a large number of tiny liquid droplets in the channel. This highly turbulent mist flow results in a substantial rise in the heat transfer coefficient. The high speed turbulent mist flow continuously wets the heat transfer wall and significantly reduces the resistance of heat transfer from the channel wall to the flow. At a higher mass flux, the mist flow is at a higher velocity and the heat transfer is better (Yan et al., 1999).

In traditional test facilities, the refrigerant is heated by an electrical resistance wire wound around the tube or by direct electrical heating of the tube itself and the heat flux is controlled by the electrical power dissipated. Instead, in the present test facilities, the refrigerant inside the plate side is heated by hot water flowing counter-currently in the shell side (which corresponds more closely to the real situation in a water chiller evaporator). The effect of average heat flux on the evaporation heat transfer is shown Fig. 6 by plotting the measured data for $q_w''=4$, 6 and 8 kW/m^2 at $G=60$ kg/m^{2}s and $T_{r,sat}=10$℃ as a function of x_m. It is well known that the evaporation rate is almost proportional to the heat flux, but the present results indicate that the heat flux does not show significant effects on the evaporation heat transfer coefficient. Compared with the mass flux effects shown Fig. 5, the heat flux has a small effect on the evaporation heat transfer coefficient in the whole vapor quality region.

The effect of refrigerant saturation temperature on the evaporation heat transfer coefficient is illustrated in Fig. 7 by plotting the data for $T_{r,sat}=0$, 5 and 10℃ at $G=60$ kg/m^{2}s and $q_w''=6.0$ kW/m^2 as a function of x_m. The results suggest that at a given saturation temperature the evaporation heat transfer coefficient increases with the mean vapor quality. At a fixed x_m, the evaporation heat transfer coefficient is lower for a higher $T_{r,sat}$ in the whole quality region. Specifically, the mean heat transfer coefficient at 0℃ is about 20% larger than that at 10℃. This is attributed to the lower specific volume of R-134a vapor at a higher saturation temperature, which, in turn, causes lower vapor flow rate and hence lower shear force to the liquid film on the heat transfer surface. Moreover, the latent heat of vaporization is smaller for higher R-134a saturation temperature.

It is necessary to compare the present data for the R-134a evaporation heat transfer coefficient to those for the plate heat exchanger reported in the literature. Due to the limited availability of the data for plate heat exchangers with the same range of parameters covered in the present study, the comparison is only possible for a few cases. This is illustrated in Fig. 8, in which our data are compared with correlation of Yan et al. (1999). Note that the correlation from Yan et al.

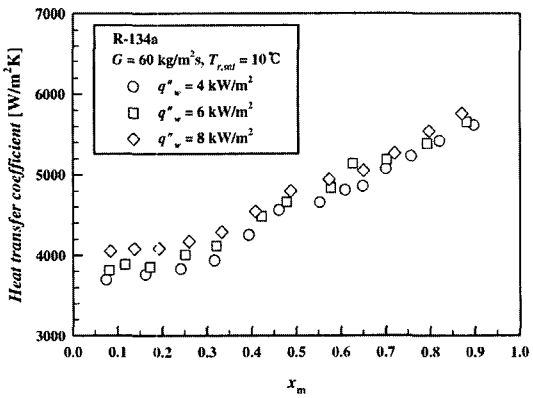

Fig. 6 Variation of evaporation heat transfer coefficient with mean vapor quality for various heat fluxes at $G=60$ kg/m^{2}s and $T_{r,sat}=10$℃

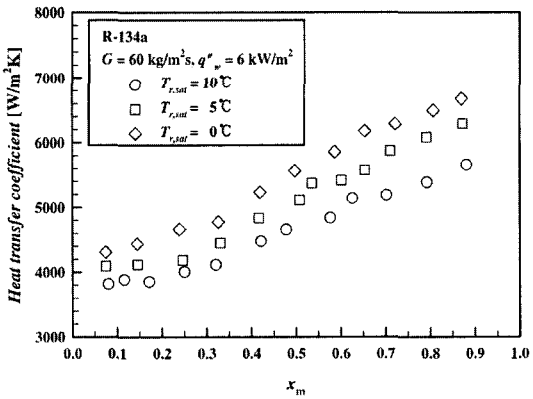

Fig. 7 Variation of evaporation heat transfer coefficient with mean vapor quality for various saturation temperatures at $G=60$ kg/m^{2}s and $q_w''=6$ kW/m^2

are based on average evaporation heat transfer coefficient measured in a plate heat exchanger with the vapor quality from about 0.1 to 0.9. Yan et al. proposed evaporation heat transfer correlation equation such as

$$\left(\frac{h_r D_h}{k_l}\right) \mathrm{Pr}_l^{-1/3} \mathrm{Re}^{0.5} Bo_{eq}^{-0.3} = 1.926 \mathrm{Re}_{eq} \quad \text{for } 2000 < \mathrm{Re}_{eq} < 10000 \tag{21}$$

where Re_{eq} and Bo_{eq} are, respectively, the equivalent Reynolds and Boiling numbers defined as

$$\mathrm{Re}_{eq} = \frac{G_{eq} D_h}{\mu_l} \tag{22}$$

$$Bo_{eq} \equiv \frac{q''}{G_{eq} \cdot i_{fg}} \tag{23}$$

Here, G_{eq} was proposed by Akers et al.(1958) and is an equivalent mass flux which is a function of the mass flux, mean quality and densities at the saturated condition. The comparison shows that the R-134a evaporation heat transfer coefficient for oblong shell and plate heat exchanger is about 35% in average higher than that for the plate heat exchanger.

4.3 Two phase frictional pressure drop

Figure 9 shows the effect of the refrigerant mass flux on R-134a frictional pressure drop. The results indicate that at a given mass flux the pressure drop is larger for a higher vapor quality. In addition, the pressure drop with the vapor quality is more pronounced for a higher mass flux. This obviously results from the simple fact that at a higher x_m the velocity of vapor was larger and the pressure drop was thus higher.

Figure 10 shows the effects of the heat flux on the frictional pressure drop. The data indicate that at a given heat flux the frictional pressure drop increases linearly with the mean vapor quality of the refrigerant. But the heat flux dose not show significant effect on the frictional pressure drop.

It is known that for a higher saturation temperature, the specific volume of the vapor and

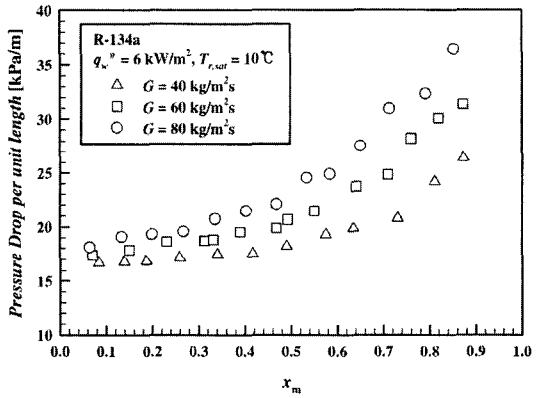

Fig. 9 Frictional pressure drop variations with the mean vapor quality for various mass fluxes at q_w''=6.0 kW/m² and $T_{r,sat}$=10℃

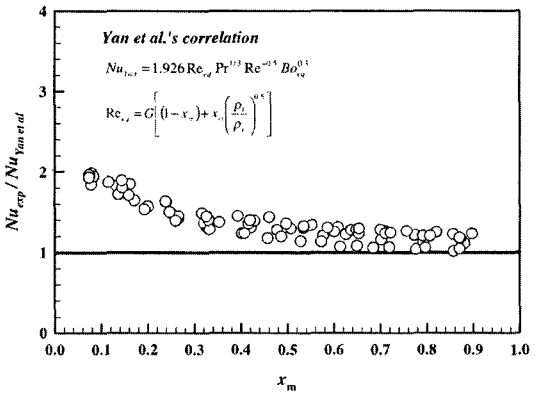

Fig. 8 Comparison of the present heat transfer data with those for plate heat exchanger from Yan et al.(1999)

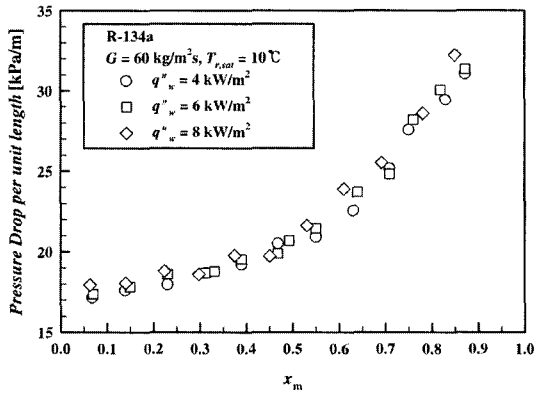

Fig. 10 Frictional pressure drop variations with the mean vapor quality for various heat fluxes at G=60 kg/m²s and $T_{r,sat}$=10℃

the viscosity of the liquid R-134a are lower. Thus, the results in Fig. 11 for different saturation temperatures of R-134a indicate that in the total vapor quality range the pressure drop is lower at a higher $T_{r,sat}$. Note that at a given $T_{r,sat}$ the pressure drop is larger for a higher vapor quality.

Figure 12 shows the comparison of Yan et al.'s pressure drop correlation to the present data. Yan et al. proposed evaporation pressure drop correlation equation such as

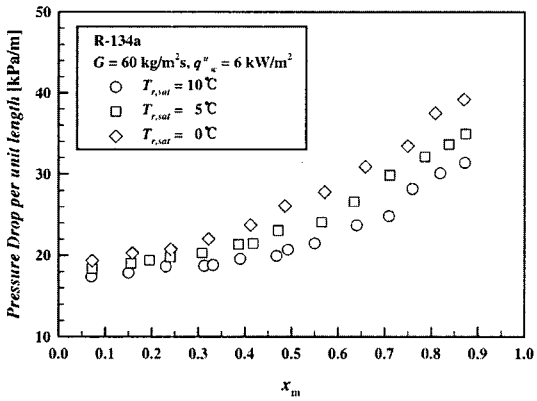

Fig. 11 Frictional pressure drop variations with the mean vapor quality for various saturation temperatures at G=60 kg/m²s and q_w''=6.0 kW/m²

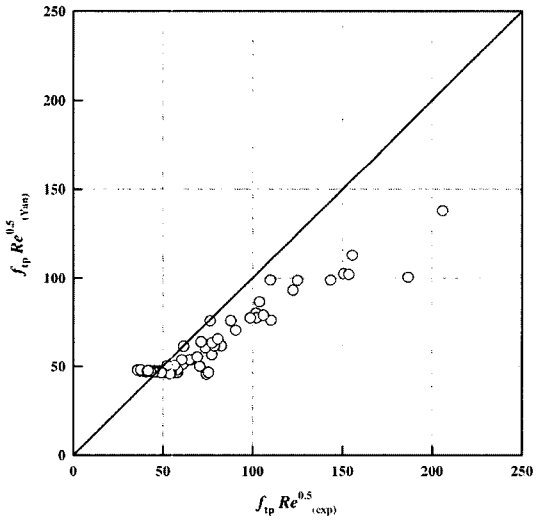

Fig. 12 Comparison of the present pressure drop data with those for plate heat exchanger from Yan et al.(1999)

$$f_{tp}\mathrm{Re}^{0.5}=6.947\times10^{5}\mathrm{Re}_{eq}^{-1.109},\ \mathrm{Re}_{eq}<6000$$
$$=31.21\mathrm{Re}_{eq}^{0.04557},\ \mathrm{Re}_{eq}\geq6000 \quad (24)$$

The comparison shows that the R-134a evaporation pressure drop for oblong shell and plate heat exchanger is about 15% in average higher than that for plate heat exchanger.

4.4 Correlation equations

To facilitate the use of oblong shell and plate heat exchanger as evaporators, correlating equations for the dimensionless evaporation heat transfer coefficient and friction factor based on the present data are provided. These are the modified forms of Yan et al.'s correlations.

$$Nu=12.47\mathrm{Re}_{eq}^{0.33}\mathrm{Pr}_{l}^{1/3},\ 1700<\mathrm{Re}_{eq}<12500 \quad (25)$$

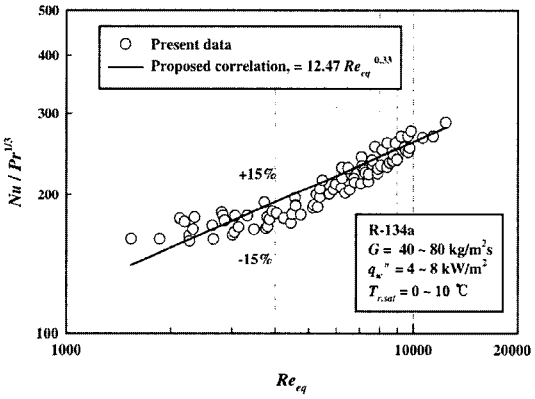

Fig. 13 Comparison of the proposed correlation for Nusselt number with the present data

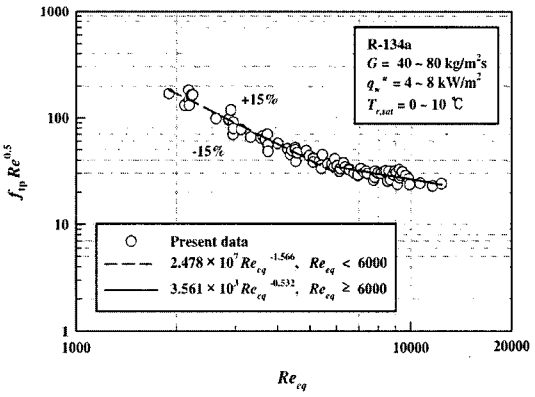

Fig. 14 Comparison of the proposed correlation for friction factor with the present data

and

$$f_{tp}\mathrm{Re}^{0.5}=2.478\times10^{7}\mathrm{Re}_{eq}^{-1.566},\ \mathrm{Re}_{eq}<6000$$
$$=3.561\times10^{3}\mathrm{Re}_{eq}^{-0.532},\ \mathrm{Re}_{eq}\geq6000 \quad (26)$$

Figure 13 shows the comparison of the proposed evaporation heat transfer correlation to the present data, indicating that most of the experimental values are within ±15%. Figure 14 shows the comparison of the proposed correlation for the friction factor to the present data. It is found that the average deviation is about ±15% between f_{tp} correlation and the data.

5. Conclusions

An experiment has been carried out in the present study to measure the heat transfer coefficients and pressure drops for the evaporation of R-134a flowing in the oblong shell and plate heat exchanger. The effects of the mass flux, average imposed heat flux, saturation temperature and vapor quality on the measured data were experimentally examined.

The present results show that the evaporation heat transfer coefficients and pressure drops normally increase with the refrigerant mass flux. The heat flux does not show significant effects both on the evaporation heat transfer coefficients and frictional pressure drops for the whole vapor quality. It was noted that, at a higher saturation temperature, evaporation heat transfer coefficients and pressure drops are lower.

In addition, the present data for the R-134a evaporation heat transfer coefficients and pressure drops were compared with those in the plate heat exchanger reported in the literature. The comparison shows that both the evaporation heat transfer coefficients and pressure drops for oblong shell and plate heat exchanger is higher than those for the plate heat exchanger. We further note that the rise in the evaporation heat transfer coefficient is more pronounced than that in the pressure drop.

Finally, the empirical correlations are also provided for the measured heat transfer coefficients and pressure drops in terms of the Nusselt number and friction factor.

Acknowledgment

This work has been supported by Regional Research Center for Advanced Environmentally Friendly Energy Systems of Pukyong National University.

References

Akers, W. W., Dean, H. A. and Crosser, O., 1958, "Condensation Heat Transfer Within Horizontal Tubes," *Chem. Eng. Prog.*, 54, pp. 89~90.

Farrell, P., Wert, K. and Webb, R., 1991, "Heat Transfer and Friction Characteristics of Turbulent Radiator Tubes," *SAE Technical Paper series*, No. 910197.

Kline, S. J. and McClintock, F. A., 1953, "Describing Uncertainties in Single-sample Experiments," *Mechanical Engineering*, Vol. 75, No. 1, pp. 3~12.

Shah, R. K. and Focke, W. W., 1988, "Plate Heat Exchangers and Their Design Theory," in: Shah, R. K., Subbarao, E. C., Mashelkar, R. A. (eds.), Heat Transfer Equipment Design, Hemisphere, Washington, DC, pp. 227~254.

Shah, R. K. and Wanniarachchi, A. S., 1992, "Plate Heat Exchanger Design Theory in Industry Heat Exchanger," in: J. M. Buchlin (eds.), Lecture Series, No, 1991-04, Von Karman Institute for Fluid Dynamics, Belgium.

Sieder, E. N. and Tate, G. E., 1936, "Heat Transfer and Pressure Drop of Liquids in Tubes," *Int. Eng. Chem.*, Vol. 28, pp. 1429~1435.

Wilson, E. E., 1915, "A Basis for Rational Design of Heat Transfer Apparatus," *Trans. ASME*, Vol. 37, pp. 47-70.

Yan, Y. -Y. and Lin, T. -F., 1999, "Evaporation Heat Transfer and Pressure drop of Refrigerant R-134a in a Plate Heat Exchanger," *J. Heat Transfer*, Vol. 121, pp. 118~127.

Zivi, S. M., 1964, "Estimation of Steady State Void Fraction by means of the Principle of Minimum Entropy Production," *Trans. Am. Soc. Mech. Eng., Ser. C. J. Heat Transfer*, Vol. 86, pp. 247~252.